

Chiral high-harmonic generation in metasurfaces

Piyush Jangid,¹ Maria Antonietta Vincenti,²

Luca Carletti,² Yuri Kivshar,¹ and Sergey Kruk³

¹*Research School of Physics, Australian National
University, Canberra ACT 2601 Australia*

²*Department of Information Engineering,
University of Brescia, 25123 Brescia, Italy*

³*ARC Centre of Excellence QUBIC, IBMD,
School of Mathematical and Physical Sciences,
University of Technology Sydney Ultimo, NSW 2007, Australia**

Abstract

High-harmonic generation (HHG) provides the only source of attosecond pulses with the currently shortest accessible time intervals, and it is employed as the only table-top source of light in extreme UV and soft X-ray spectral regions. Chiral HHG can be employed as an efficient tool for studying the ultrafast response of chiral properties of matter, as well as for amplifying chiroptical effects. Traditionally, chiral high harmonics were associated with gases of enantiomer molecules or, more recently, solid surfaces with helicity in their crystalline structure. Here, we bring the concept of chiral high-harmonic generation to nanophotonics, specifically to metasurfaces consisting of arrays of nanoresonators. Our system is achiral at the material and individual nanoresonators. Chirality rises and falls in a controlled manner via an interplay of the nanoresonator symmetry and the symmetry of the metasurface lattice. Our calculations predict up to 10^8 contrast in harmonic brightness between the two orthogonal circular polarizations of the pump. Our findings at the intersection of chiral nanophotonics and strong-field optics pave the way for chiral attosecond physics and chiral extreme UV optics in nanostructured solids.

I. INTRODUCTION

High-harmonics generation (HHG) has traditionally been associated with gases [1] and plasma [2], and more recently it entered the realm of solid-state physics [3]. Solid-state sources are attractive for broadening the range of HHG applications to create smaller, simpler, and cheaper systems. However, bulky solids hinder some of the key applications of HHG as the source of attosecond pulses or source of ultrashort wavelengths: short-wavelength radiation, such as extreme ultraviolet (UV) radiation, is being absorbed rapidly in the bulk solids, and ultrafast pulses are being distorted by the material dispersion.

This opens up a unique niche for HHG in ultra-thin, nanostructured solids – nanoresonators [4] and metasurfaces [5]. The ultra-thin form-factor mitigates the disadvantages of bulky solids, while the judicious design of the metasurfaces at the nanoscale can enhance the efficiency of light-matter interactions by orders of magnitude via an engineered resonant response [6, 7].

Chiral metasurfaces have been employed in linear optics as well as in the generation of low-order (2^{nd} and 3^{rd}) optical harmonics. Chirality in metasurfaces may emerge from (i) symmetry group of the material at the microscopic level, e.g., at the level of atomic lattice, (ii) symmetry group of an individual nanoresonator/unit cell, (iii) symmetry breaking by the oblique incidence of light (termed extrinsic chirality), (iv) symmetry group of a lattice of nanoresonators, (v) interplays between all above. [8–16]

Nonlinear chirality of up to the third order has been demonstrated for the resonant excitation of the metasurface with circularly polarized light [12], to probe the maximal chiroptical response [17, 18] and uncover novel applications, such as ultra-fast switching of light polarizations [19, 20], chiral sensing by anapole modes [21], generation of spin unlocked vortex beam [22], multiplexed holography [23], and logic gates [24]. However, the expansion of chirality to strong-field optics and to the HHG regime, although known in gases [25, 26] and unstructured solids [27–29], has not yet been explored in optical nanostructures, including metasurfaces.

In this paper, we study numerically a nonlinear metasurface made of properly oriented achiral nanoresonators and reveal that it shows a very strong nonlinear chirality contrast up to, at least, the fifth harmonics. Moreover, we show that nonlinear resonant chiral response is equally present for several different sources of nonlinearities, including nonlinearities arising from bulk, dipolar contributions, or from symmetry breaking at the surface of the resonators. Our results suggest the generation of even and odd optical harmonics down to the UV spectral range, where amorphous silicon

possesses significant absorption, and they pave the way for advanced polarization control of HHG with nanofabrication technologies.

II. METASURFACE DESIGN

We consider an amorphous silicon (Si)-on-fused silica (SiO_2) metasurface consisting of achiral nanoresonators inside a square lattice, as shown in Fig. 1b. Individual resonators are discs with notches, and the orientation of the notch with respect to the metasurface lattice is denoted by the angle of the notch θ (Fig. 1a). When θ points along one of the lattice symmetry axes, shown as dashed lines in Fig. 1a, the periodic array preserves the mirror symmetry and, thus, is achiral. However, for other values of θ , the resonator and substrate break mirror symmetry along all geometric axes, which consequently induces chirality in metasurfaces with achiral resonators at normal incidence. In other words, the notch angle of the individual resonators acts as a knob that allows to easily control the degree of chirality of the metasurfaces.

First, we simulate numerically the linear chiral response of the metasurface with COMSOL Multiphysics by considering a lattice spacing of $P = 975 \text{ nm}$, a nanoresonator radius of $R = 452.5 \text{ nm}$, a height of $H = 245 \text{ nm}$, a notch size of $(r, s) = (52.5 \text{ nm}, 420 \text{ nm})$ and a notch angle of $\theta = 57^\circ$ with respect to the x axis. Figure 1c shows the metasurface transmission when the left circularly polarized (LCP) light and right circularly polarized light (RCP) light illuminate the metasurface at normal incidence, labeled T_L and T_R , respectively. For metasurfaces, linear chirality is usually measured in terms of circular dichroism, which is the differential transmission of LCP and RCP [9, 12]. However, its conventional definition involves absorption instead of transmission [30]. So we refrain from explicitly using the term circular

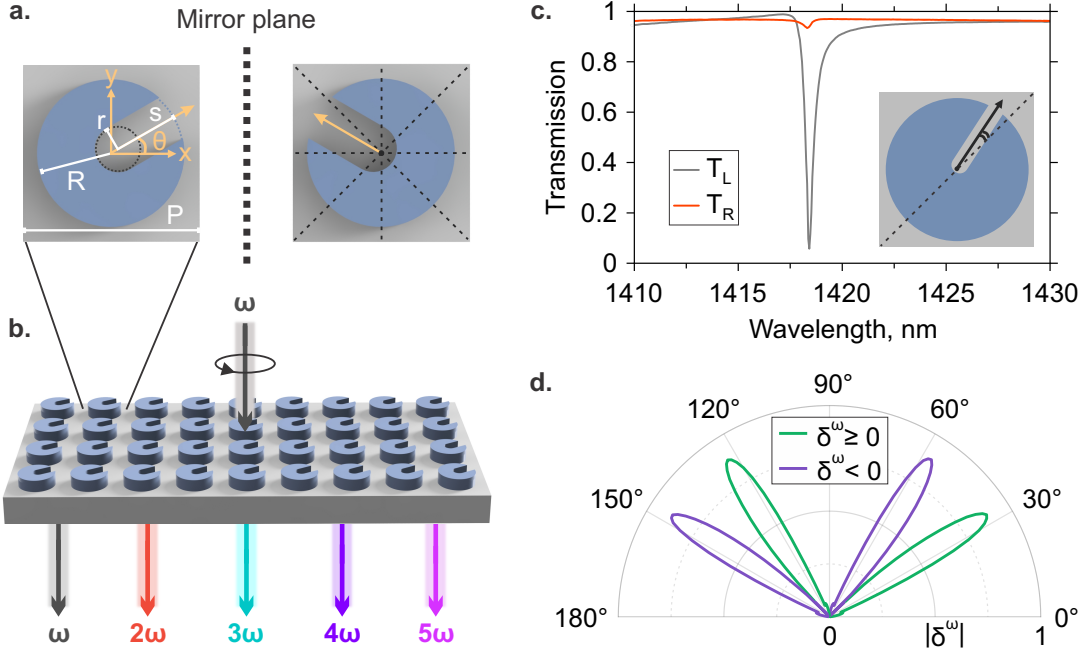


Figure 1. **a.** Schematic of achiral nanoresonators arranged in a square lattice. The notations for characteristic dimensions are shown. Dashed lines are the square lattice mirror symmetry planes, and θ is the notch angle. **b.** Concept of the metasurface generating chiral high-harmonics from the second (2ω) to fifth (5ω) order at the incident circularly polarized pump ω . **c.** Linear transmission spectrum metasurface for incident LCP and RCP, denoted as T_L and T_R , respectively. (inset) The unit cell of the designed metasurface. **d.** Variation of linear chirality (δ^ω) in the vicinity of the resonance with the notch angle.

dichroism and instead quantify linear chirality by the parameter δ^ω , defined as

$$\delta^\omega = \frac{(T_L - T_R)}{(T_L + T_R)}, \quad (1)$$

which gives rise to $|\delta^\omega| \approx 0.88$ at the resonance. Next, we study the interplay between resonator orientation and metasurface chirality. By fine-tuning θ , while keeping the

other geometrical parameters the same, we observe a change in the chiral response of the metasurface (δ^ω): the chiral response ranges from a minimum on the lattice symmetry planes when $\theta = 0^\circ, 45^\circ$ and 90° , to the extrema at 33° and 57° , in the first quadrant (see Fig. 1d). The same behavior repeats in the remaining quadrants (not shown).

III. NONLINEAR CHIRAL RESPONSE

To analyze the nonlinear behavior of the metasurface, we implemented a numerical model that combines the effective second-order response that arises from symmetry breaking at the surface and bulk third-order nonlinearity. Silicon has a centrosymmetric crystal structure[31], therefore, it does not show any second-order bulk nonlinearity in either its crystalline or amorphous form. As a result, the only second-order nonlinear sources present in the resonators originate from volume and surface contributions that arise from magnetic dipoles (Lorentz force), inner-core electrons, convective nonlinear sources, and electron gas pressure [32–36]. To take into account all these nonlinear terms, we solve the electromagnetic problem at the second-harmonic frequency as outlined in Refs. [37, 38].

In particular, second-harmonic current density sources are calculated as the superposition of two terms: a volume term, J_{vol} , and a surface term, J_{surf} . We then include these two currents into a finite element solver where the five harmonics are mutually coupled as described in the Supplementary Information, while the bulk third-order nonlinear susceptibility, assumed to be isotropic, is included with a dispersion profile calculated according to Miller’s rule [39, 40] (see Supplementary Information for more details on the implementation of the model). We calculate the transmitted second, third, fourth and fifth harmonic conversion efficiencies for both LCP and RCP pump as the transmitted power at each frequency, normalized by the incident pump

power P_{FF} , where $P_{FF} = I_{FF} \cdot P$, where P is the periodicity of the metasurface and $I_{FF} = 50 \text{ MW/cm}^2$ is the pump irradiance. We stress that we use a relatively low pump irradiance value so that the contribution of higher-order nonlinearities, namely $\chi^{(5)}$ and $\chi^{(7)}$, can be neglected.

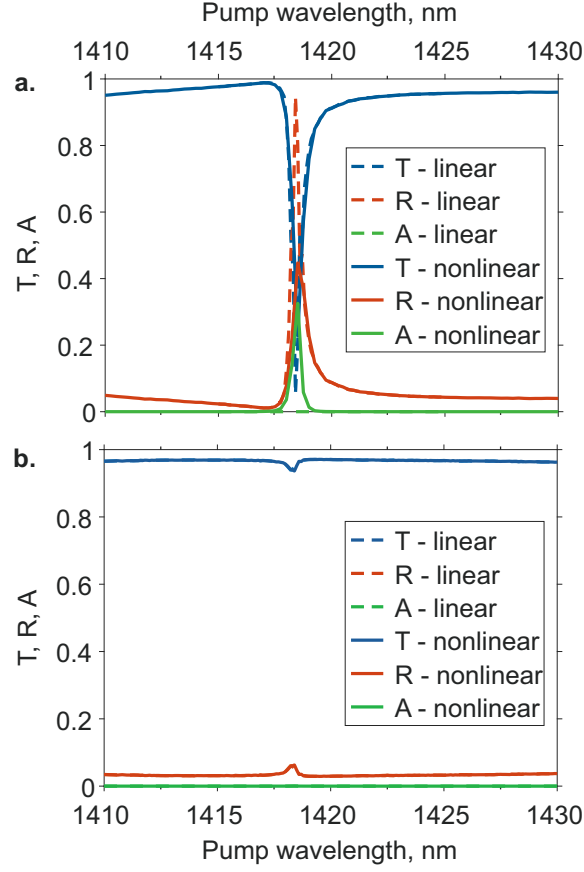


Figure 2. **a.** Linear (dashed lines - pump intensity $I_{FF} = 1 \text{ W/cm}^2$) and nonlinear (solid lines - pump intensity $I_{FF} = 50 \text{ MW/cm}^2$) transmission, reflection, and absorption for LCP incident light **b.** same as in a. for RCP incident light.

Figures 2a,b summarize our results for linear vs. nonlinear transmission, reflection, and absorption of the metasurfaces for the two orthogonal circular polarizations,

where nonlinear transmission/reflection accounts for the modulation of the epsilon by the pump (see Sec. III of Supplementary Information).

Conversion efficiencies for both even and odd harmonics are shown in Fig. 3a for the two cases of illumination: with LCP (solid lines) and RCP (dashed lines), and for the $\theta = 57^\circ$ degree angle corresponding to the maximum of chirality. We contrast this calculation to Fig. 3b where $\theta = 45^\circ$. We stress that, although the strength of the nonlinear response for all harmonics is significantly different for the two polarizations, the second harmonic is more efficient than the third harmonic, and the fourth harmonic is stronger than the fifth harmonic, despite their inherently different origin. This can be attributed to the tensorial form of amorphous silicon that naturally suppresses odd harmonic generation under circularly polarized light [41] illumination and the electric field localization profile at the resonant pump frequency that boosts second-order nonlinear processes arising from symmetry breaking at the surface of the disks (see Supplementary Information for electric and magnetic field distribution in the nanodisk resonator). We perform a control calculation of harmonics generation from a plain Si film of thickness identical to the metasurface height, at normal incidence and for linear polarisation (see Fig. 3c). In this case, the response is dominated by the third harmonic, which becomes brighter than the second harmonic as is conventionally expected from the bulk nonlinearities of silicon. Correspondingly, for the thin film, the fifth harmonic also becomes brighter than the fourth harmonic.

In our calculations, down-conversion effects have also been included because of the high local fields that are achieved at the resonance wavelength. The impact of the feedback at the pump frequency is particularly evident for LCP excitation, with a nonlinear transmission that is modestly affected by the nonlinear interactions and nonlinear absorption that increases dramatically at the expense of nonlinear reflection. On the other hand, under RCP illumination, no significant changes are

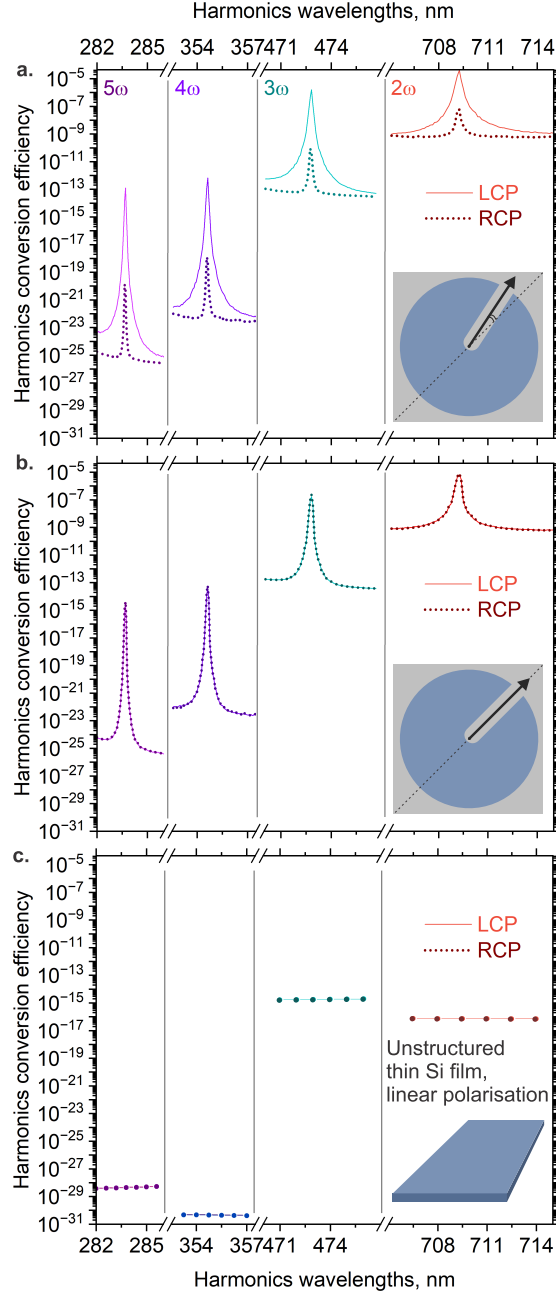


Figure 3. **a.** Second-to-fifth harmonic conversion efficiencies for LCP (solid lines) and RCP (dashed lines) incident light and the notch angle of 57° . **b.** Same as **a.** for the notch angle of 45° . **c.** Control calculation of harmonics generation from plain Si film at normal incidence for linearly polarized pump

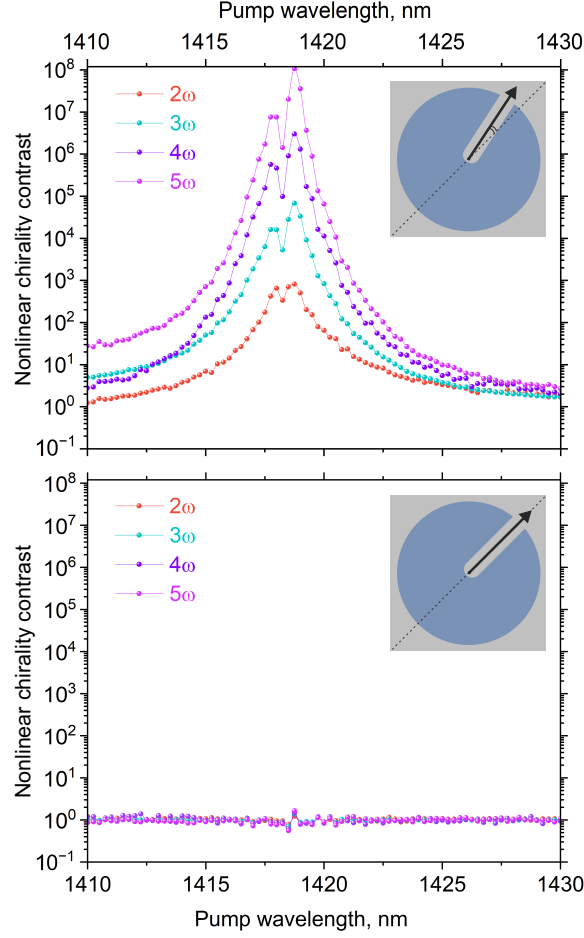


Figure 4. **a.** Contrast of harmonics generation efficiency for LCP versus RCP excitation for the notch angle of 57° . **b.** Same as **a.** for the notch angle of 45° .

registered going from a low-intensity linear regime ($I_{FF} = 1 \text{ W/cm}^2$) to the nonlinear regime ($I_{FF} = 50 \text{ MW/cm}^2$).

For a comparison of harmonics brightness between the two orthogonal circular polarizations of pump, we define nonlinear chirality contrast as

$$\frac{I_L^{n\omega}}{I_R^{n\omega}} \quad (2)$$

where $I_L^{n\omega}$ ($I_R^{n\omega}$) is the intensity of n^{th} -harmonic generation for incident LCP (RCP) pump. Our calculations predict a nonlinear chirality contrast of up to 10^8 for the optimal notch angle θ (see Fig.4a). The control calculation for the θ angle corresponding to the achiral case shows no chirality contrast (see Fig.4b). Interestingly, outside the resonance, we see the harmonic signal several orders of magnitude stronger than in the film. This is because the disks have a slightly higher electric field inside as compared to the film.

Finally, we calculate nonlinear chirality, quantified by $\delta^{n\omega}$, as

$$\delta^{n\omega} = \frac{I_L^{n\omega} - I_R^{n\omega}}{I_L^{n\omega} + I_R^{n\omega}} \quad (3)$$

The $\delta^{n\omega}$ at resonance is $> 99.9\%$ for 4^{th} and 5^{th} harmonics, $> 99.7\%$ for 2^{nd} and 3^{rd} harmonics. To provide evidence that the chiral nonlinear dynamics is enabled by the specific notch angle, we compare the chirality contrast of the studied metasurface with the one from a metasurface with $\theta = 45^\circ$ and get the achiral response in the latter case.

IV. CONCLUSION

Our study provides a theoretical demonstration of the chiral generation of multiple optical harmonics, including the harmonics of both even and odd orders. This phenomenon arises because of the intricate interplay between the point symmetries of the unit cell and those of the overall lattice structure of the metasurface. By carefully engineering these symmetries at the nanoscale, we have established a robust mechanism for inducing chirality in nonlinear optical processes, even in materials that are intrinsically achiral at the atomic level. Our findings reveal the fundamental role of nanoscale structures in tailoring and enhancing chiral responses in strong-field

light-matter interactions, offering a powerful alternative to relying solely on naturally chiral materials, which may be limited in availability or optical performance. Instead, our results suggest that conventional material platforms can be transformed into highly efficient chiral optical media through precise nanostructuring. Beyond its fundamental significance, our work paves the way towards practical applications of chiral photonics, including ultrafast spectroscopy and the development of novel light sources with tailored polarization properties. Moreover, the ability to achieve strong chiral effects through structured solids opens exciting opportunities in many areas such as quantum optics, optical information processing, and the control of light-matter interactions at extreme field intensities.

ACKNOWLEDGEMENTS

SK acknowledges financial support from the Australian Research Council (grant DE210100679). MAV and LC acknowledge financial support from the NATO Science for Peace and Security program (Grant no. 5984). YK was supported by the Australian Research Council (Grant No. DP210101292) and the International Technology Center Indo-Pacific (ITC IPAC) via Army Research Office (contract FA520923C0023).

SUPPLEMENTARY INFORMATION

See Supplementary Information for supporting content.

* Corresponding author: sergey.kruk@uts.edu.au

- [1] M. Ferray, A. L’Huillier, X. F. Li, L. A. Lompre, G. Mainfray, and C. Manus, Multiple-harmonic conversion of 1064 nm radiation in rare gases, *Journal of Physics B: Atomic, Molecular and Optical Physics* **21**, L31 (1988).
- [2] N. H. Burnett, H. A. Baldis, M. C. Richardson, and G. D. Enright, Harmonic generation in co2 laser target interaction, *Applied Physics Letters* **31**, 172 (1977), https://pubs.aip.org/aip/apl/article-pdf/31/3/172/18435123/172_1_online.pdf.
- [3] S. Ghimire and D. A. Reis, High-harmonic generation from solids, *Nature Physics* **15**, 10.1038/s41567-018-0315-5 (2018).
- [4] A. Zalogina, L. Carletti, A. Rudenko, J. V. Moloney, A. Tripathi, H.-C. Lee, I. Shadrivov, H.-G. Park, Y. Kivshar, and S. S. Kruk, High-harmonic generation from a subwavelength dielectric resonator, *Science Advances* **9**, eadg2655 (2023), <https://www.science.org/doi/pdf/10.1126/sciadv.adg2655>.
- [5] P. Jangid, F. U. Richter, M. L. Tseng, I. Sinev, S. Kruk, H. Altug, and Y. Kivshar, Spectral tuning of high-harmonic generation with resonance-gradient metasurfaces, *Advanced Materials* **36**, 2307494 (2024), <https://advanced.onlinelibrary.wiley.com/doi/pdf/10.1002/adma.202307494>.
- [6] S. Kruk and Y. Kivshar, Functional meta-optics and nanophotonics governed by mie resonances, *ACS Photonics* **4**, 2638 (2017), <https://doi.org/10.1021/acsp Photonics.7b01038>.
- [7] V. Zubyuk, L. Carletti, M. Shcherbakov, and S. Kruk, Resonant dielectric metasurfaces in strong optical fields, *APL Materials* **9**, 060701 (2021), https://pubs.aip.org/aip/apm/article-pdf/doi/10.1063/5.0048937/19761367/060701_1_5.0048937.pdf.

- [8] S. S. Kruk, C. Helgert, M. Decker, I. Staude, C. Menzel, C. Etrich, C. Rockstuhl, C. Jagadish, T. Pertsch, D. N. Neshev, and Y. S. Kivshar, Optical metamaterials with quasicrystalline symmetry: Symmetry-induced optical isotropy, *Phys. Rev. B* **88**, 201404 (2013).
- [9] S. S. Kruk, A. N. Poddubny, D. A. Powell, C. Helgert, M. Decker, T. Pertsch, D. N. Neshev, and Y. S. Kivshar, Polarization properties of optical metasurfaces of different symmetries, *Phys. Rev. B* **91**, 195401 (2015).
- [10] C. Menzel, C. Rockstuhl, and F. Lederer, Advanced jones calculus for the classification of periodic metamaterials, *Phys. Rev. A* **82**, 053811 (2010).
- [11] I. Brener, S. Liu, I. Staude, J. Valentine, and C. L. Holloway, eds., in *Dielectric Metamaterials* (Elsevier, 2020) Chap. 5, p. 165.
- [12] K. Koshelev, P. Tonkaev, and Y. Kivshar, Nonlinear chiral metaphotonics: a perspective, *Advanced Photonics* **5**, 064001 (2023).
- [13] A. Nikitina, A. Nikolaeva, and K. Frizyuk, Nonlinear circular dichroism in achiral dielectric nanoparticles, *Phys. Rev. B* **107**, L041405 (2023).
- [14] I. Toftul, P. Tonkaev, K. Koshelev, F. Lai, Q. Song, M. Gorkunov, and Y. Kivshar, Chiral dichroism in resonant metasurfaces with monoclinic lattices, *Phys. Rev. Lett.* **133**, 216901 (2024).
- [15] I. Sinev, F. U. Richter, I. Toftul, N. Glebov, K. Koshelev, Y. Hwang, D. G. Lancaster, Y. Kivshar, and H. Altug, Chirality encoding in resonant metasurfaces governed by lattice symmetries (2024), arXiv:2412.20955 [physics.optics].
- [16] I. Toftul, D. Hariharan, P. Tonkaev, F. Lai, Q. Song, and Y. Kivshar, Monoclinic nonlinear metasurfaces for resonant engineering of polarization states (2025), arXiv:2501.08494 [physics.optics].
- [17] Y. Tang, Z. Liu, J. Deng, K. Li, J. Li, and G. Li, Nano-kirigami metasurface with giant nonlinear optical circular dichroism, *Laser & Photonics Reviews* **14**, 2000085

- (2020), <https://onlinelibrary.wiley.com/doi/pdf/10.1002/lpor.202000085>.
- [18] T. Shi, Z.-L. Deng, G. Geng, X. Zeng, Y. Zeng, G. Hu, A. Overvig, J. Li, C.-W. Qiu, A. Alù, Y. S. Kivshar, and X. Li, Planar chiral metasurfaces with maximal and tunable chiroptical response driven by bound states in the continuum, *Nature Communications* **13**, 4111 (2022).
 - [19] L. Kang, C.-Y. Wang, X. Guo, X. Ni, Z. Liu, and D. H. Werner, Nonlinear chiral metamirrors: Enabling technology for ultrafast switching of light polarization, *Nano Letters* **20**, 2047 (2020), pMID: 32031817, <https://doi.org/10.1021/acs.nanolett.0c00007>.
 - [20] H. Wang, Z. Hu, J. Deng, X. Zhang, J. Chen, K. Li, and G. Li, All-optical ultrafast polarization switching with nonlinear plasmonic metasurfaces, *Science Advances* **10**, eadk3882 (2024), <https://www.science.org/doi/pdf/10.1126/sciadv.adk3882>.
 - [21] G. Serrera, J. González-Colsa, and P. Albella, Amplified linear and nonlinear chiral sensing assisted by anapole modes in hybrid metasurfaces, *Applied Physics Letters* **124**, 251701 (2024), <https://pubs.aip.org/aip/apl/article-pdf/doi/10.1063/5.0212393/20002616/251701.1.5.0212393.pdf>.
 - [22] M. Wang, R. Rong, J. Chen, H. Xu, K. Li, G. Li, and S. Chen, Spin unlocked vortex beam generation on nonlinear chiroptical metasurfaces, *Nano Letters* **24**, 3654 (2024), pMID: 38498929, <https://doi.org/10.1021/acs.nanolett.3c04922>.
 - [23] X. Hong, K. Wang, C. Guan, X. Han, Y. Chen, S. Qian, X. Xing, C.-W. Qiu, and P. Lu, Chiral third-harmonic metasurface for multiplexed holograms, *Nano Letters* **22**, 8860 (2022), pMID: 36346747, <https://doi.org/10.1021/acs.nanolett.2c02283>.
 - [24] Y. Zhang, Y. Wang, Y. Dai, X. Bai, X. Hu, L. Du, H. Hu, X. Yang, D. Li, Q. Dai, T. Hasan, and Z. Sun, Chirality logic gates, *Science Advances* **8**, eabq8246 (2022), <https://www.science.org/doi/pdf/10.1126/sciadv.abq8246>.
 - [25] A. Fleischer, O. Kfir, T. Diskin, P. Sidorenko, and O. Cohen, Spin angular momentum and tunable polarization in high-harmonic generation, *Nature Photonics* **8**, 543 (2014).

- [26] O. Kfir, P. Grychtol, E. Turgut, R. Knut, D. Zusin, D. Popmintchev, T. Popmintchev, H. Nembach, J. M. Shaw, A. Fleischer, H. Kapteyn, M. Murnane, and O. Cohen, Generation of bright phase-matched circularly-polarized extreme ultraviolet high harmonics, *Nature Photonics* **9**, 99 (2015).
- [27] N. Saito, P. Xia, F. Lu, T. Kanai, J. Itatani, and N. Ishii, Observation of selection rules for circularly polarized fields in high-harmonic generation from a crystalline solid, *Optica* **4**, 1333 (2017).
- [28] N. Klemke, O. D. Mücke, A. Rubio, F. X. Kärtner, and N. Tancogne-Dejean, Role of intraband dynamics in the generation of circularly polarized high harmonics from solids, *Phys. Rev. B* **102**, 104308 (2020).
- [29] T. Heinrich, M. Taucer, O. Kfir, P. B. Corkum, A. Staudte, C. Ropers, and M. Sivilis, Chiral high-harmonic generation and spectroscopy on solid surfaces using polarization-tailored strong fields, *Nature Communications* **12**, 3723 (2021).
- [30] P. W. Atkins and J. De Paula, *The elements of physical chemistry*, 4th ed. (Oxford University Press, London, England, 2005).
- [31] P. Patnaik, *Handbook of inorganic chemicals*, Vol. 529 (McGraw-Hill New York, 2003).
- [32] E. Adler, Nonlinear optical frequency polarization in a dielectric, *Physical Review* **134**, A728 (1964).
- [33] N. Bloembergen, R. K. Chang, S. Jha, and C. Lee, Optical second-harmonic generation in reflection from media with inversion symmetry, *Physical Review* **174**, 813 (1968).
- [34] M. Scalora, J. Trull, C. Cojocaru, M. Vincenti, L. Carletti, D. de Ceglia, N. Akozbek, and C. De Angelis, Resonant, broadband, and highly efficient optical frequency conversion in semiconductor nanowire gratings at visible and uv wavelengths, *JOSA B* **36**, 2346 (2019).
- [35] M. Scalora, M. A. Vincenti, D. de Ceglia, V. Roppo, M. Centini, N. Akozbek, and M. Bloemer, Second-and third-harmonic generation in metal-based structures, *Physi-*

- cal Review A **82**, 043828 (2010).
- [36] K. Hallman, L. Rodríguez-Suné, J. Trull, C. Cojocaru, M. A. Vincenti, N. Akozbek, R. Vilaseca, and M. Scalora, Harmonic generation from silicon membranes at visible and ultraviolet wavelengths, *Optics express* **31**, 792 (2023).
 - [37] M. A. Vincenti, S. Campione, D. de Ceglia, F. Capolino, and M. Scalora, Gain-assisted harmonic generation in near-zero permittivity metamaterials made of plasmonic nanoshells, *New Journal of Physics* **14**, 103016 (2012).
 - [38] D. de Ceglia, S. Campione, M. A. Vincenti, F. Capolino, and M. Scalora, Low-damping epsilon-near-zero slabs: Nonlinear and nonlocal optical properties, *Physical Review B* **87**, 155140 (2013).
 - [39] R. C. Miller, Optical second harmonic generation in piezoelectric crystals, *Applied Physics Letters* **5**, 17 (1964).
 - [40] R. Boyd, *Nonlinear optics*, academic, San Diego, Calif **1992**, 39 (2008).
 - [41] C. L. Tang and H. Rabin, Selection rules for circularly polarized waves in nonlinear optics, *Phys. Rev. B* **3**, 4025 (1971).

Supplementary Information: Chiral high-harmonics generation in metasurfaces

I. LINEAR PERMITTIVITY RESPONSE

Amorphous silicon experimental data are shown in Fig.S1.

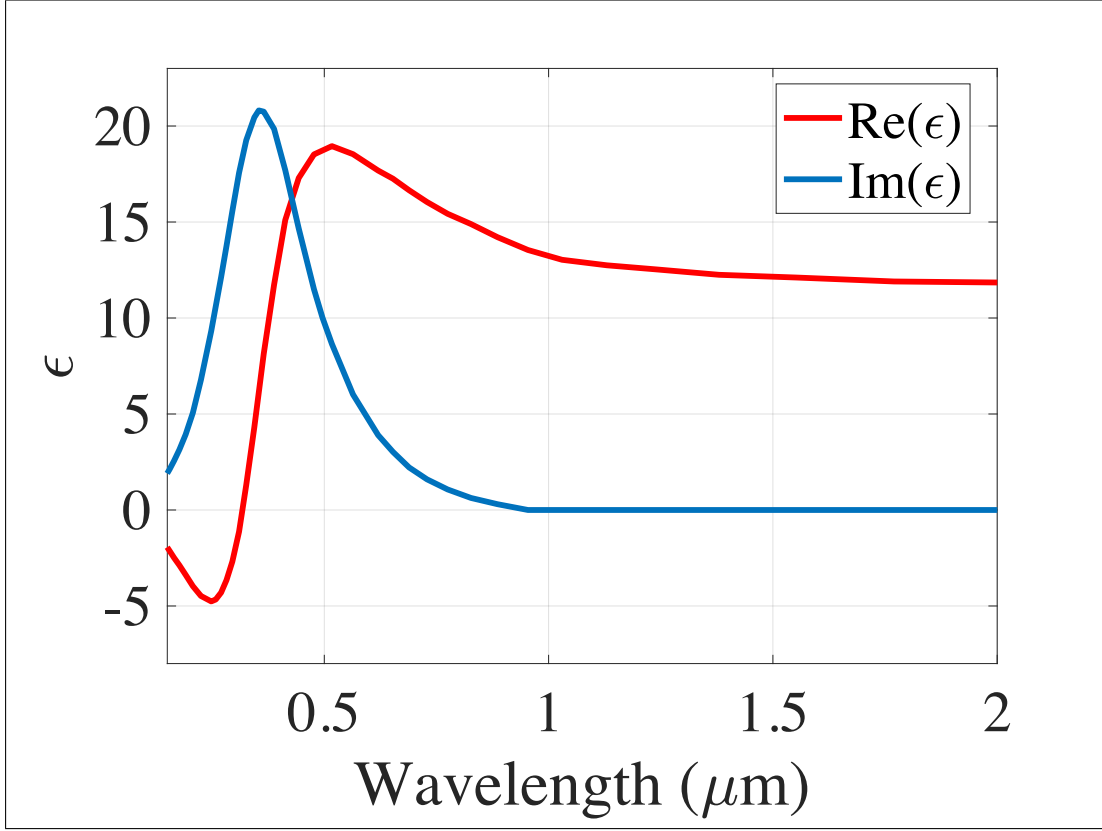


Figure 1.

II. ELECTRIC FIELD DISTRIBUTION

Electric field enhancement, calculated as $|E|/E_0$, where E_0 is the incident electric field calculated at the resonance wavelength $\lambda = 1418 \text{ nm}$ for LCP (Fig. S2 a) and RCP (Fig. S2 b). We note that the electric field is strongly localized at the surface

of the nanodisks, boosting even harmonic generation that arises from symmetry breaking at the interfaces.

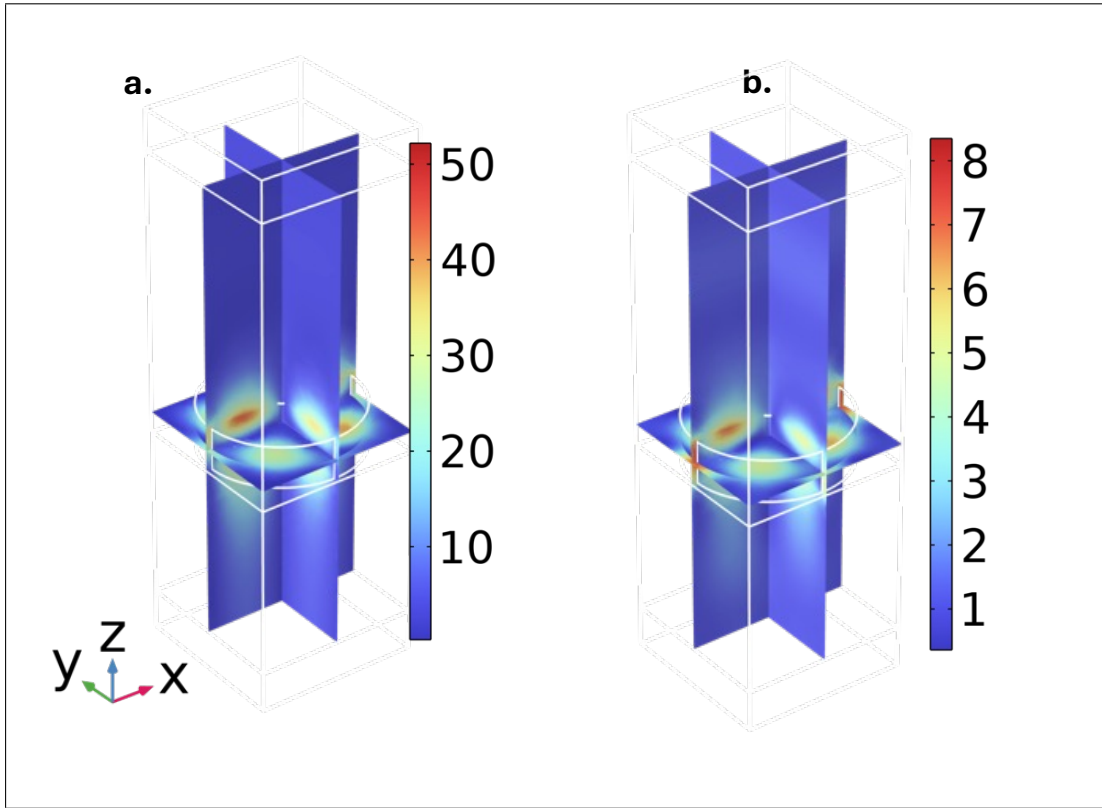


Figure 2.

III. SECOND ORDER NONLINEAR RESPONSE

Second order nonlinear currents are linked to the fundamental frequency (FF) electric field and to the material parameters as follows:

$$\hat{\mathbf{n}} \cdot \mathbf{J}_s = i \frac{n_0 e^3}{2m_b^*} \frac{3 + \varepsilon_{FF}}{(\omega + i\gamma_0)^2 (2\omega + i\gamma_0)} E_{FF,\perp}^2 \quad (1)$$

$$\hat{\mathbf{t}} \cdot \mathbf{J}_s = i \frac{n_0 e^3}{2m_b^*} \frac{1}{(\omega + i\gamma_0)^2 (2\omega + i\gamma_0)} E_{FF,\perp} E_{FF,\parallel} \quad (2)$$

$$\begin{aligned} \mathbf{J}_v = & i \frac{n_0 e^3}{2m_b^*} \frac{1}{\omega(\omega + i\gamma_0)(2\omega + i\gamma_0)} \\ & \left[\frac{\gamma_0}{\omega + \gamma_0} (\mathbf{E}_{FF} \cdot \nabla) \mathbf{E}_{FF} - \frac{i}{2} \nabla (\mathbf{E}_{FF} \cdot \mathbf{E}_{FF}) \right] \end{aligned} \quad (3)$$

where $n_0 = \varepsilon_0 m_b^{*2} \omega_p^2 / e^2$ is the bound electrons density, the effective bound electron mass is assumed equal to the electron mass $m_b^* = m_e = 9.10938188 \times 10^{-31}$ kg, e is the elementary charge, and the plasma frequency, ω_p , and decay rate, γ_0 , used to fit the dielectric permittivity of amorphous silicon are $\omega_p = 1.6953 \times 10^{16}$ rad/s and $\gamma_0 = 2.4487 \times 10^{15}$ rad/s, respectively. The value of the permittivity ε_{FF} of Si at the FF, ω is the angular frequency of the FF field, \mathbf{E}_{FF} is the FF electric field phasor, and $\hat{\mathbf{n}}$ and $\hat{\mathbf{t}}$ are unit vectors pointing in directions outward normal and tangential to the nanodisk surface, respectively. Moreover, $\mathbf{E}_{FF,\perp}$ and $\mathbf{E}_{FF,\parallel}$ are the normal and tangential components of the FF electric field in the local boundary coordinate system defined by $\hat{\mathbf{n}}$ and $\hat{\mathbf{t}}$, and are evaluated inside the Si resonator regions.

IV. IMPLEMENTATION OF THE FIVE HARMONICS MODEL

We developed a five-harmonics model to evaluate the conversion efficiencies of the metasurface made of Si nanodisks. To simplify the computational approach we calculate two different dispersion profiles for the third-order nonlinear susceptibility tensor, one that catches the nonlinear processes occurring at frequencies between the

pump and the second harmonic described by $\chi^{(3)i,j,k,l}(\omega; \omega, \omega, -\omega)$, while the other is associated with processes occurring from the third to the fifth harmonics described by $\chi^{(3)i,j,k,l}(3\omega; \omega, \omega, \omega)$ where $ijkl$ are cartesian axes. Since we assume the nanodisk to be made of amorphous silicon, we consider tensorial elements corresponding to an isotropic response [S1]. Because of the high field localization values reached in the silicon resonators, we also include pump depletion, self- and cross-phase modulation processes between all harmonics, discarding those terms that contain powers of the second or higher harmonics. This results into the following nonlinear polarization terms at the pump and harmonic frequencies:

$$P_{\omega,i}^{NL} = \chi_{ijkl}^{(3)} \left[(3E_{\omega,j}|E_{\omega,j}|^2 + 2E_{\omega,j}|E_{\omega,k}|^2 + 2E_{\omega,j}|E_{\omega,l}|^2 + E_{\omega,j}^* (E_{\omega,k}^2 + E_{\omega,l}^2)) \right] \quad (4)$$

$$P_{2\omega,i}^{NL} = \chi_{ijkl}^{(3)} \left[6E_{2\omega,j}|E_{\omega,j}|^2 + 2E_{2\omega,j}|E_{\omega,k}|^2 + 2E_{2\omega,j}|E_{\omega,l}|^2 \right] + \\ \chi_{ijkl}^{(3)} \left[2E_{2\omega,k} (E_{\omega,j}^* E_{\omega,k} + E_{\omega,k}^* E_{\omega,j}) + 2E_{2\omega,l} (E_{\omega,j}^* E_{\omega,l} + E_{\omega,l}^* E_{\omega,j}) \right] + \\ \chi_{ijkl}^{(3)} \left[E_{4\omega,j} (3E_{\omega,j}^{*2} + E_{\omega,k}^{*2} + E_{\omega,l}^{*2}) + 2E_{\omega,j}^* (E_{4\omega,k} E_{\omega,k}^* + E_{4\omega,l} E_{\omega,l}^*) \right] \quad (5)$$

$$P_{3\omega,i}^{NL} = \chi_{ijkl}^{(3)} E_{\omega,j} (E_{\omega,j}^2 + E_{\omega,k}^2 E_{\omega,l}^2) \quad (6)$$

$$P_{4\omega,i}^{NL} = \chi_{ijkl}^{(3)} \left[E_{2\omega,j} (3E_{\omega,j}^2 + E_{\omega,k}^2 + E_{\omega,l}^2) + 2E_{\omega,j} (E_{2\omega,k} E_{\omega,k} + E_{2\omega,l} E_{\omega,l}) \right] + \\ \chi_{ijkl}^{(3)} \left[E_{4\omega,k} (6|E_{\omega,j}|^2 + 2|E_{\omega,k}|^2 + 2|E_{\omega,l}|^2) + \right. \\ \left. 2E_{4\omega,k} (E_{\omega,j}^* E_{\omega,k} + E_{\omega,k}^* E_{\omega,j} + E_{\omega,j}^* E_{\omega,l} + E_{\omega,l}^* E_{\omega,j}) \right] \quad (7)$$

$$P_{5\omega,i}^{NL} = \chi_{ijkl}^{(3)} \left[E_{3\omega,j} (3E_{\omega,j}^2 + E_{\omega,k}^2 + E_{\omega,l}^2) + E_{\omega,j} (2E_{3\omega,k} E_{\omega,k} + 2E_{3\omega,l} E_{\omega,l}) \right] \quad (8)$$

V. REFERENCES

S1. R. Boyd, San Diego, Calif 19922, 39 (2008).